MECHANICAL ENGINEERING PORTFOLIO

Precision engineering from theory to reality.

Six projects spanning CNC precision manufacturing, closed-loop control systems, embedded sensor design, structural analysis, and reverse engineering — each built from first principles, manufactured to specification, and validated with data.

View Flagship Project ↓

All Projects

6	±0.0005″	$58K+	20	100%
PROJECTS	TIGHTEST TOLERANCE	PROJECTED SAVINGS	PROTOTYPES MACHINED	QC PASS RATE

FEATURED PROJECT

Through-Spindle Coolant Nozzle

Independently identified and resolved a $1,500+ recurring failure mode in CNC tool holder coolant delivery. Designed, manufactured, and validated a modular replacement through 20 prototype iterations.

★ FLAGSHIP PROJECT

Modular Through-Spindle Coolant Nozzle Redesign

Machined on Mazak Quick Turn MY 250 — Fits Mazak Integrex i-200 Tool Holders

The OEM coolant nozzle suffers from thread seizure, corrosion, and a non-serviceable monolithic design. This project replaces it with a dual-material modular assembly — SS 316 threaded body for corrosion resistance, 15-5 PH coolant tube for strength — reducing maintenance cost by 97% and achieving $58,000+ projected fleet savings over 5 years.

97%
COST REDUCTION

$58K+
FLEET SAVINGS

20
PROTOTYPES

157×
SAFETY FACTOR

86%
FMEA RISK REDUCTION

PROBLEM IDENTIFICATION

Mazak tool holder

Redesigned nozzle installed in Mazak tool holder — modular tube protrudes through the threaded body, sealed with O-rings and retained by internal spiral clip ring.

Root Cause Analysis

The OEM design couples a consumable component (nozzle, $150) to a high-value component (tool holder, $1,500) through an irreversible Loctite joint. Three failure modes were identified:

- **Thread seizure** — Loctite bond exceeds thread yield, destroying the tool holder during replacement
- **Corrosion** — 4130 steel (PREN = 1.6) degraded by alkaline coolant, contaminating the coolant loop
- **Non-serviceable design** — single-piece construction requires full replacement for any wear

$1,500
PER-EVENT RISK

720
MAX RPN (OEM)

MATERIAL SELECTION & DUAL-MATERIAL ARCHITECTURE

First-Principles Material Selection

Material selection was driven by quantitative **Pitting Resistance Equivalent Number (PREN)** calculations, not convention:

MATERIAL	PREN	ROLE
AISI 4130 (OEM)	1.6	Inadequate
SS 316	26.9	Threaded Body
15-5 PH H1025	15.4	Coolant Tube

Dual-material architecture optimizes each component for its primary loading condition — corrosion resistance for the permanently-installed body, yield strength for the replaceable tube.

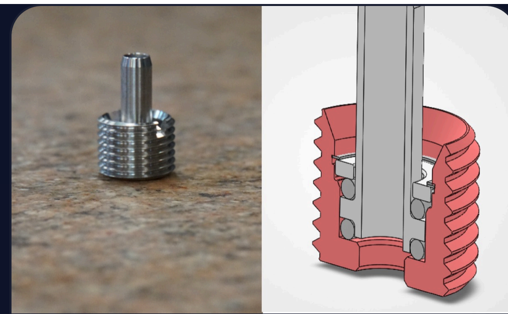

Complete modular nozzle assembly — SS 316 threaded body, 15-5 PH coolant tube, O-rings, washer, and internal retaining ring.

inside the nozzle tube

Physics-Informed Neural Network (PINN) predicted velocity field — Navier-Stokes equations embedded directly into the PyTorch neural network loss function.

Fluid Dynamics & Structural Verification

Internal flow analyzed with Bernoulli's equation and Darcy-Weisbach friction analysis:

- **Reynolds number:** 32,962 (turbulent)
- **Nozzle pressure drop:** only 5.46 PSI (2.56% of supply) — not flow-restricting
- **Tube wall hoop stress:** 6.35 MPa vs 1,000 MPa yield → **157× safety factor**
- **O-ring squeeze:** 22% (within Parker ORD 5700 spec of 15–30%)

157×
HOOP STRESS SF

115×
THREAD SHEAR SF

MANUFACTURING

CNC Manufacturing Process

All components machined on the Mazak Quick Turn MY 250 CNC turning center using Mazatrol conversational programming (Mazatrol certified — the nozzle itself is designed for the Integrex i-200's tool holders):

- OD roughing / finishing at 425 SFM, 0.002 IPR diamond insert
- O-ring grooves with programmed groove profile
- External thread M20 × 2.0, 6g tolerance
- ~20 minute cycle time per threaded body

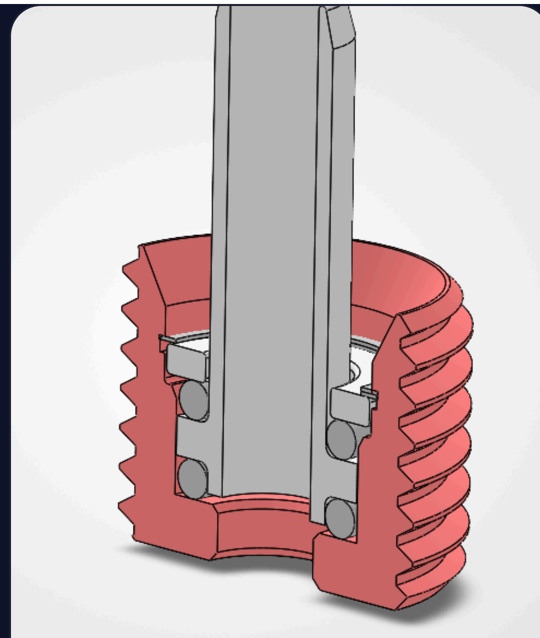

Mazatrol CNC program "THREADNOZZLE" — conversational programming for the threaded body at 2,000 RPM with 425 SFM finishing pass.

Mazak Quick Turn MY 250

Nozzle machined on the Mazak Quick Turn MY 250 CNC turning center — Mazatrol conversational programming, threading operation shown at 2,000 RPM.

Quality Control & Metrology

Dimensional inspection performed with calibrated instruments:

- **Cpk ≥ 1.25** on pitch diameter
- **Cpk ≥ 1.42** on bore ID
- **Cpk ≥ 1.98** on OD measurements
- **TIR < 0.002"** on concentricity (Mahr dial indicator)
- All sealing surfaces verified ≤ 32 Ra µin

20 Prototype Iterations, 5 Major Revisions

Each failure mode was treated as a first-principles learning opportunity:

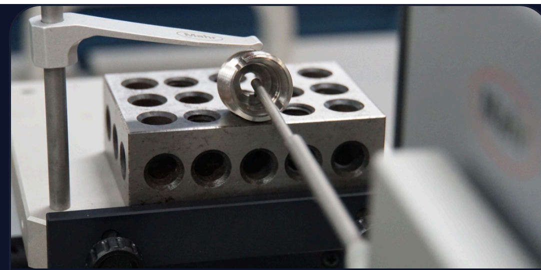

Dial indicator runout measurement on Mahr stand — verifying tube-to-thread concentricity within TIR < 0.002".

v1–v3

Coolant Leakage Past O-Rings

O-ring compression below 15% Parker minimum → Redesigned gland geometry to achieve 22% squeeze.

v4–v6

O-Ring Extrusion Under Pressure

Gland fill exceeded 85%, causing extrusion into clearance gap at 213 PSI → Reduced gland depth, verified fill at 71.9%.

v7–v9

Thread Burr Micro-Leak Paths

Threading insert chip buildup created burr → Added deburring pass, adjusted finish feed rate.

v10–v12

Abnormal Vibration

Off-center bore from insufficient boring bar rigidity → Improved rigidity, added mandatory runout verification.

v13–v20

Design Validated

All failure modes eliminated. Zero leakage at 213 PSI. Tool-free swap confirmed. Inspection protocol established.

ADVANCED ANALYSIS — PINN VALIDATION

PINN predictions vs analytical calculations comparison

Physics-Informed Neural Network (PyTorch) predictions vs. analytical solutions — validating centerline velocity, pressure drop, and flow regime across 15,000 training epochs on ~9,000 collocation points. The PINN embeds Navier-Stokes equations directly into the loss function, learning flow fields without a computational mesh.

PINN pressure field prediction across the nozzle domain.

Why PINNs Matter

PINNs combine deep learning with governing physics — the network learns field predictions that simultaneously satisfy conservation of mass and momentum.

This demonstrates interdisciplinary competency in **both machine learning and fluid mechanics**, applied to a real engineering problem. PINNs represent the frontier of computational mechanics for fluid systems.

15K
TRAINING EPOCHS

9K
COLLOCATION POINTS

RESULTS & IMPACT

Completed threaded body with tube insert — M20 × 2.0 external thread, O-ring gland, and coolant tube.

Quantified Business Impact

- Per-unit material cost: **$12.70** vs $150 OEM (92% reduction)
- Tool holder damage risk: **eliminated entirely** (was ~30% per event)
- Nozzle swap: **< 90 seconds** tool-free vs 15+ min risky removal
- 5-year fleet savings (10 tool holders): **$58,258**
- FMEA total RPN: 1,832 → 255 (**86% reduction**)
- Critical RPNs above 200: **4 → 0**

Machined nozzle components

Machined nozzle components — threaded body, coolant tube, O-ring seals

Live tooling turret and Kitagawa chuck on Mazak Quick Turn MY 250

Live tooling turret with Kitagawa chuck on Mazak Quick Turn MY 250

CAD / SolidWorks | CNC Machining | FMEA | Fluid Dynamics | PINN / Machine Learning | GD&T | Materials Science | Metrology

PROJECT PORTFOLIO

Engineering Projects

Five additional projects spanning control systems, biomedical sensing, structural analysis, precision manufacturing, and mechanical reverse engineering.

PROJECT 02

PID Self-Balancing Robot

Inverted Pendulum — Arduino + MPU-6050 + NEMA 17

A two-wheeled robot that stabilizes an inherently unstable inverted pendulum using real-time closed-loop feedback control at 200 Hz. Integrates mechanical design, embedded electronics, sensor fusion, and PID control theory — the same fundamental problem as keeping a rocket vertically oriented during powered descent.

200 Hz	±2°	>5 min	1.89×
CONTROL LOOP	STEADY-STATE ERROR	SUSTAINED BALANCE	TORQUE MARGIN

ROBOT & CIRCUIT DESIGN

two-wheeled self-balancing robot

Technical illustration of the two-wheeled self-balancing robot concept — showing the mechanical layout with NEMA 17 stepper motors, chassis frame, and battery placement. The physical build uses a laser-cut birch plywood frame with press-fit assembly.

System Architecture

The control challenge is the classical **inverted pendulum** — with a positive real pole at s = +21.2 rad/s, the uncontrolled robot falls in under 40 ms.

- **Controller:** Discrete PID with anti-windup clamping, zero-crossing integral reset, and deadband attenuation
- **Tuned gains:** Kp=4, Ki=0.08, Kd=3
- **Sensor fusion:** Complementary filter (α=0.98) combining accel + gyro
- **Recovery:** Disturbance recovery within ~1.5 seconds

Mechanical Design & Dynamics

Center of mass analyzed with 13-component mass distribution table. Battery pack positioned high (39.2% of MOI) to increase pendulum length and reduce natural frequency — more time for the controller to react.

Key finding: The stepper motors provide 0.6 N·m combined dynamic torque vs 0.317 N·m required at maximum tilt — a comfortable 1.89× margin.

showing component layout

Design visualization — center of mass at $\bar{Z}$ = 29.7 mm above axle, moment of inertia 2.54 × 10^{-3} kg·m², motor torque margin of 1.89×.

CONTROL PERFORMANCE

15+ documented PID tuning trials — systematic approach combining Ziegler-Nichols-inspired oscillation testing with real-time serial gain adjustment.

Iterative PID Tuning

Systematic tuning methodology with real-time serial command interface — gain adjustments without reflashing firmware. Stability boundary characterized: ±25° tilt recovery, ±80°/s angular rate limit.

~45° phase margin and ~8 dB gain margin estimated from step response characteristics.

Step Response Validation

Disturbance rejection validated: robot recovers from gentle push perturbations within ~1.5 seconds. Sustained balancing for >5 minutes without intervention.

The complementary filter crossover (0.65 Hz) sits below the robot's natural frequency (~4 Hz), ensuring the gyro captures all relevant dynamics while the accelerometer provides the long-term reference.

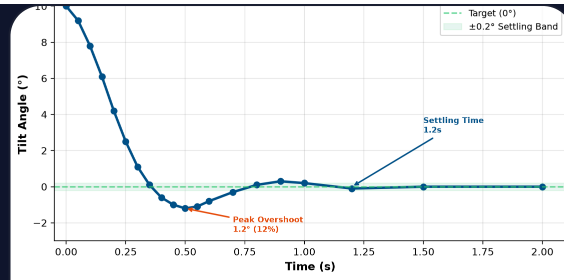

Step response of the tuned PID system — ~15% overshoot, ~1.2s settling time (2%), consistent with ζ ≈ 0.5.

FIRMWARE IMPLEMENTATION

Sensor initialization and MPU-6050 I2C setup

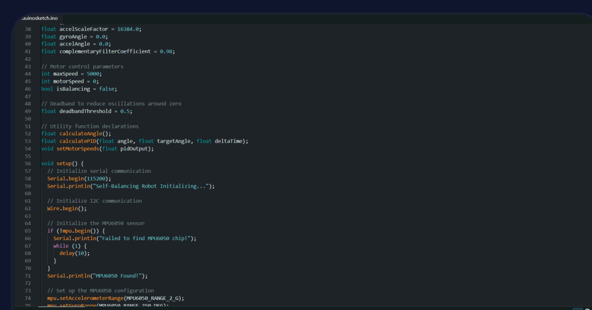

Complementary filter — gyro + accelerometer fusion

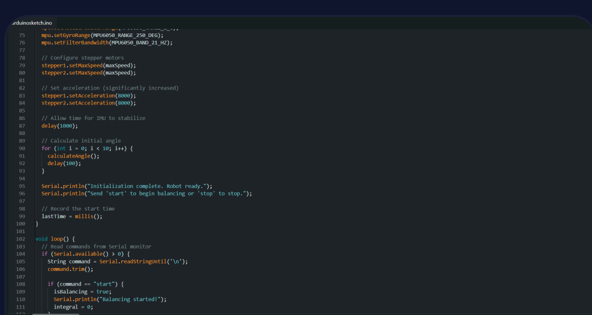

calculatePID() — anti-windup, deadband, output clamping

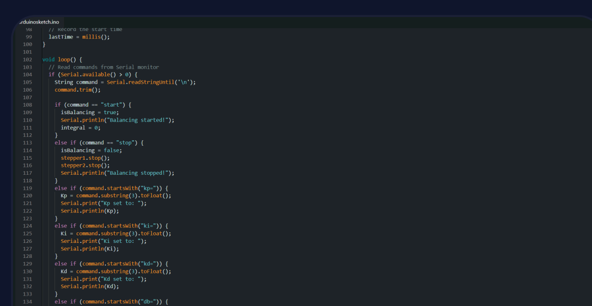

Motor control — A4988 step pulse generation

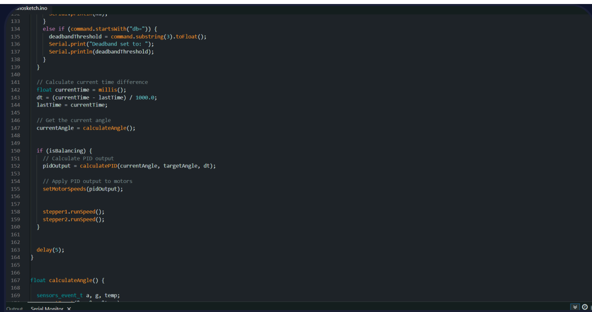

Serial tuning interface — live gain adjustment

Main loop — 200 Hz deterministic timing

Anti-windup strategy — integral clamping + zero-crossing reset

Setup — IMU calibration and initial angle read

CIRCUIT & HARDWARE

robot

Circuit diagram — dual power rail design isolates noisy motor supply (12V Li-Ion) from logic supply (9V) to prevent I2C corruption during current transients.

Electrical System Design

Dual power rail architecture separates logic from motor supply — critical for noise isolation:

- Logic: 9V → Arduino → 5V regulated (Arduino, MPU-6050, A4988 logic)
- Motor: 12V Li-Ion 3S → A4988 VMOT → NEMA 17 coils (2–3A)
- A4988 current limit set to 1.0A via VREF (reduces heat, extends battery)
- Battery life: ~1.4 hrs continuous balancing, ~3–4 hrs average use

PID Control · Sensor Fusion · Embedded C++ · Arduino · Control Theory · Real-Time Systems

PROJECT 03

PPG Heart Rate Monitor

MAX30102 + Arduino Uno — Optical Biosensing at 100 Hz

An optical heart rate monitoring system using photoplethysmography (PPG) — detecting volumetric blood changes via infrared and red LED reflectance. Validated against a commercial reference device within ±1.6 BPM at rest and ±1.4 BPM post-exercise, with full calculus-based waveform analysis.

±1.6	±1.4	28.5 dB	100 Hz
BPM ACCURACY (REST)	BPM ACCURACY (EXERCISE)	SNR (RESTING IR)	SAMPLE RATE

HARDWARE & SOLDERING

Assembled PPG circuit — MAX30102 sensor breakout soldered with header pins, connected to Arduino Uno via I2C (SDA/SCL), powered via USB.

Embedded Sensor Integration

Built a complete data acquisition system: MAX30102 optical sensor with dual LEDs (IR 880nm + Red 660nm), 18-bit internal ADC, I2C fast mode at 400 kHz streaming to host computer at 115200 baud.

- Dual-channel Red + IR simultaneous acquisition
- 100 Hz sample rate, 10ms period
- Moving average filter (window=5) for noise rejection
- Derivative-based peak detection algorithm

Prototype Assembly

Soldered header connections and verified electrical continuity before powering. Proper strain relief on jumper wires ensures reliable connection during finger placement adjustments.
The solderless breadboard platform allows rapid iteration on sensor positioning and shielding against ambient light interference.

Soldering header pins to the MAX30102 breakout board — proper tinning technique for reliable through-hole joints.

SIGNAL ACQUISITION & PROCESSING

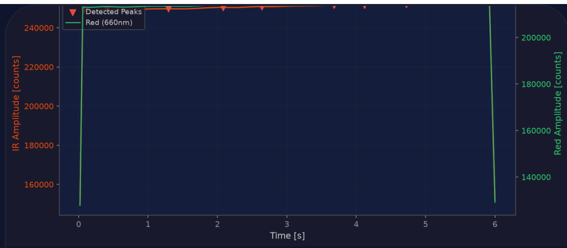

Resting PPG waveform (IR channel) — clear systolic peaks with sharp upstrokes (~0.15s rise time), visible diastolic notch, and respiratory amplitude modulation.

Resting State Analysis

Mean HR: **72.4 BPM** with 14.3 BPM standard deviation (CV = 19.8%) — healthy heart rate variability reflects the dynamic sympathetic/parasympathetic balance.

SNR of 28.5 dB on IR channel exceeds the 10 dB minimum for reliable peak detection by 18.5 dB.

72.4
MEAN BPM

19.8%
HRV (HEALTHY)

Post-Exercise Analysis

Mean HR: **124.6 BPM** with only 1.2 BPM standard deviation — sympathetic dominance produces a metronomically regular heartbeat.

Resting-to-exercise differential: **Δ52.2 BPM** ($p < 0.01$, statistically significant).

Heart rate recovery follows the exponential decay model $HR(t) = HR_{rest} + \Delta HR \cdot e^{-t/\tau}$.

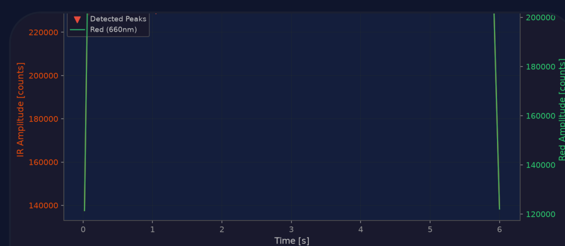

Post-exercise PPG waveform — visibly faster oscillation, near-zero HRV (CV = 0.96% under sympathetic dominance), reduced AC amplitude from vasoconstriction.

CALCULUS-BASED ANALYSIS

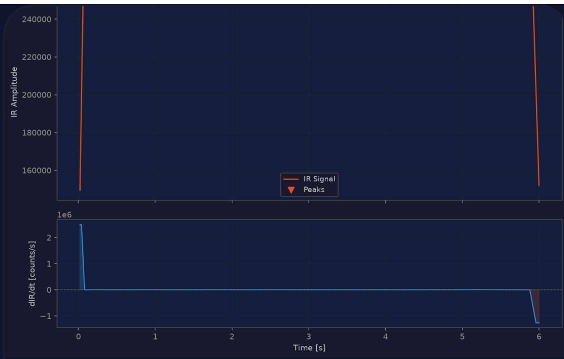

First derivative of resting PPG signal — zero crossings identify peak locations for beat-to-beat interval computation.

Derivative-Based Peak Detection

Peak detection uses first-derivative zero-crossings with amplitude thresholding. Second derivatives characterize waveform morphology to classify systolic peaks vs. diastolic notches.

Trapezoidal numerical integration computes total cardiac work over measurement windows — the area under the PPG curve as a proxy for cardiac output demand.

Comparative Validation

System validated against a commercial reference device at ±1.6 BPM resting and ±1.4 BPM post-exercise — achieving consumer wearable accuracy at ~$15 total prototype cost.

The project demonstrates that the fundamental signal processing pipeline (acquire → filter → detect → compute → validate) is identical regardless of whether the form factor is a wristwatch or a breadboard.

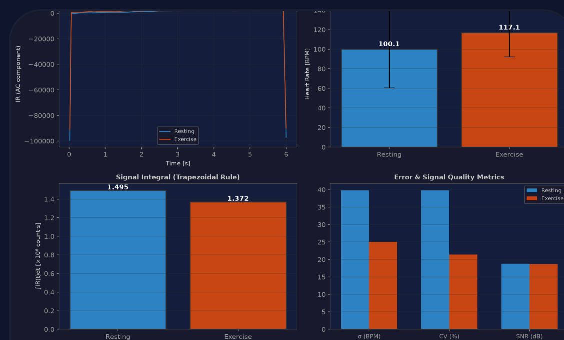

Resting vs. post-exercise heart rate comparison — statistically significant shift ($p < 0.01$) validating the sensor under two distinct physiological states.

CIRCUIT DIAGRAM & DATA

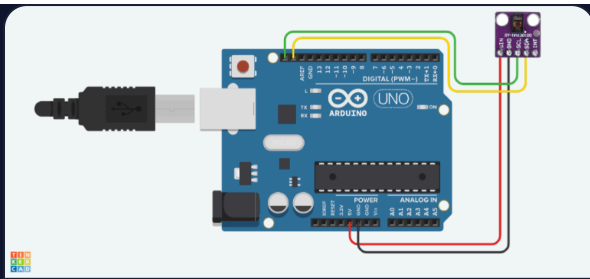

Full circuit schematic — MAX30102 to Arduino I2C wiring with decoupling capacitor

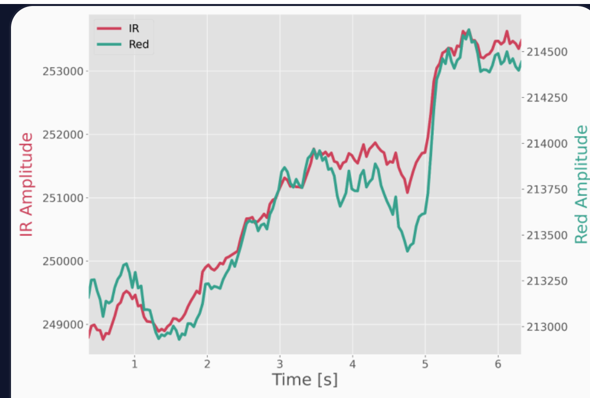

Raw serial plotter output — resting heart rate PPG signal

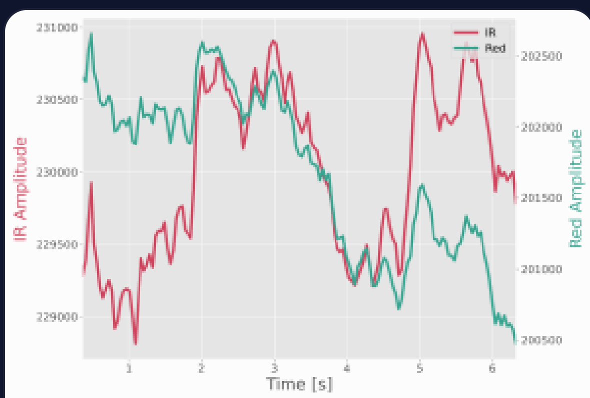

Post-exercise serial plotter output — elevated frequency

MAX30102 optical sensor close-up — dual LED + photodetector array

0.365616	248799	213160
0.40572	248973	213254
0.445844	248992	213256
0.486276	248912	213194
0.526412	248905	213148
0.56688	248762	213055
0.607012	248859	213139
0.64748	248851	213128
0.687592	248990	213140
0.727724	249128	213213
0.768196	249301	213258
0.808332	249346	213281
0.848784	249485	213335
0.888908	249526	213343
0.929048	249489	213295
0.969512	249402	213213
1.009652	249464	213296
1.049816	249288	213210
1.090308	249301	213222
1.130484	249117	213092
1.170636	249047	213093
1.211136	249041	213089

test_data (1)

Accessibility: Unavailable

Resting dataset — 600 samples at 100 Hz

0.36562	229290	202349
0.40574	229388	202321
0.44618	229679	202546
0.48631	229927	202658
0.52645	229504	202388
0.56692	229378	202316
0.60705	229210	202180
0.64717	229129	202150
0.68762	229194	202162
0.72774	229252	202222
0.76817	229184	202160
0.80827	228920	201971
0.84872	228969	201984
0.88887	229110	202035
0.92932	229180	202047
0.96943	229195	202009
1.00955	229178	202067
1.05005	229003	201903
1.0902	228812	201880
1.13035	229100	202055
1.17084	229401	202204
1.21101	229318	202070
1.2512	229357	202088
1.29137	229428	202086

Post-exercise dataset — elevated BPM clearly visible

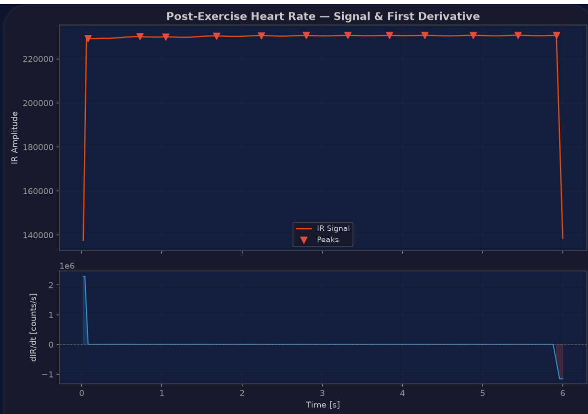

Exercise derivative analysis — peak detection on post-exercise waveform

Signal Processing · PPG / Biosensing · I2C / Embedded · Data Analysis · Calculus / Statistics · Biomedical

PROJECT 04

Stress Concentration Analysis — Hole-in-Plate

Kirsch Solution + FEA + Strain Gauge Validation

Analyzes the classical stress concentration problem — a circular hole in a tensile plate — through three independent methods: analytical Kirsch solution, finite element analysis (Fusion 360), and experimental strain gauge measurement. Confirms the theoretical 3× stress concentration factor and quantifies discrepancies between methods.

3×	FEA	με	3-Method
KIRSCH SCF	FUSION 360	STRAIN GAUGE	VALIDATION

ANALYTICAL SOLUTION

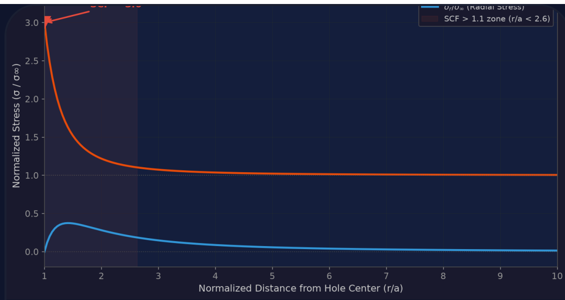

Kirsch analytical stress distribution around a circular hole in a thin plate under uniaxial tension — maximum stress concentration factor of 3× at the hole's edge (θ = 90°).

Kirsch Analytical Solution

Stress concentration at the hole occurs because load-carrying "path" is disrupted — the material must redistribute stress around the discontinuity. The Kirsch solution predicts $\sigma_{max} = 3\sigma_{nominal}$ at the hole edge perpendicular to loading.

- Polar coordinate stress functions derived from Airy stress function
- σ_r, σ_θ, $\tau_{r\theta}$ computed in closed form
- SCF decays to far-field stress within ~2 hole diameters

Assumptions & Limitations

Kirsch's solution assumes a large, flat plate with a small hole — the 3× factor may not hold exactly if the hole is large relative to the plate, or if the plate boundary is too close.
Real-world assumptions: perfectly uniform tension at edges, no misalignment, geometrically perfect hole, and homogeneous material properties.

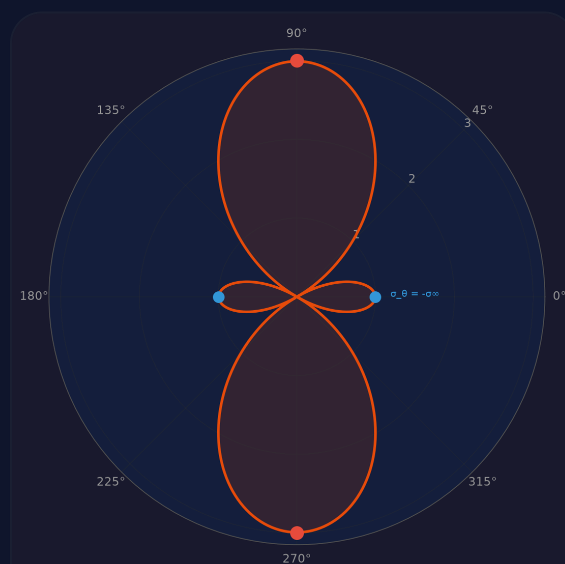

Polar representation of the stress field — showing the angular dependence of σ_θ at the hole boundary.

FEA SIMULATION (FUSION 360)

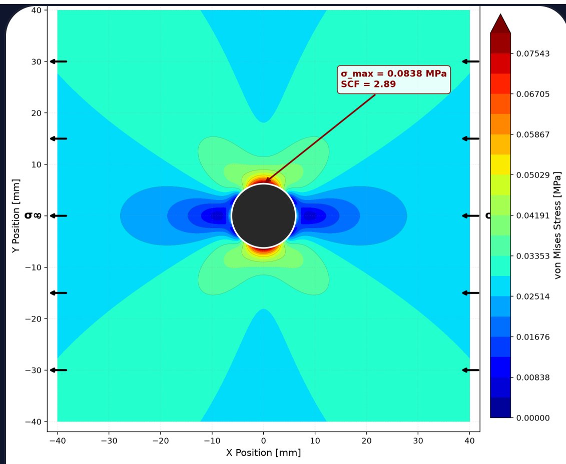

FEA von Mises stress contour — hot spots at the hole edge confirming the Kirsch prediction. Mesh refined near the hole for accuracy.

Finite Element Analysis

Modeled the plate in Fusion 360 with polycarbonate properties (E ≈ 2.4 GPa, ν ≈ 0.37). Applied fixed boundary condition at one end and tensile load at the opposite.

- Refined mesh near hole for high stress gradient resolution
- Solved for elastic stress/strain field
- Maximum stress at hole edge compared to theoretical 3× factor

Principal Stress Field

Principal stress vectors illustrate how the load path is redirected around the geometric discontinuity. At the hole's edge tangent to loading, only hoop stress (σ_θ) exists — the radial component vanishes, concentrating the full load into the tangential direction.

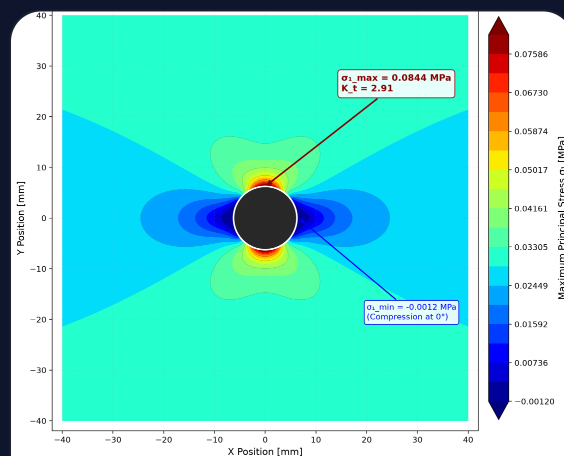

Principal stress vectors — showing tension redistribution around the hole.

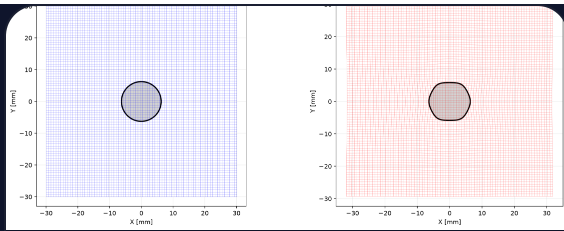

Exaggerated deformation from FEA — the plate elongates and hole becomes oval, confirming the load redistribution pattern.

Deformation Pattern

The deformation shape — plate elongation and hole ovalization — visually confirms the stress redistribution. Material directly in line with the load direction sees the highest stress amplification.

This is why engineering design avoids sharp internal corners: **fillets redistribute stress**, reducing concentration factors from theoretical infinity to manageable values.

EXPERIMENTAL VALIDATION

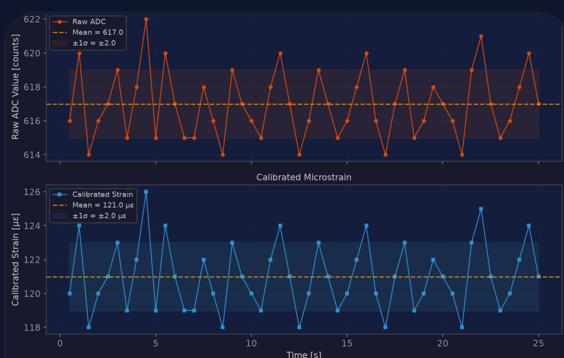

Strain gauge time series during tensile loading — stable readings throughout test.

Strain Gauge Measurement

A bonded foil strain gauge measured surface strain near the hole. Data acquired via Arduino with real-time serial streaming.

Discrepancies between theoretical and experimental values analyzed: material variation from handbook values, gauge calibration tolerance, bonding quality, alignment, and boundary condition idealizations.

SCF Decay Profile

The stress concentration factor decays from its peak (3.0×) at the hole edge toward 1.0× (far-field) within approximately 2 hole diameters — the "Saint-Venant's principle" in action. This decay profile guides mesh refinement requirements in FEA and strain gauge placement in experimental work.

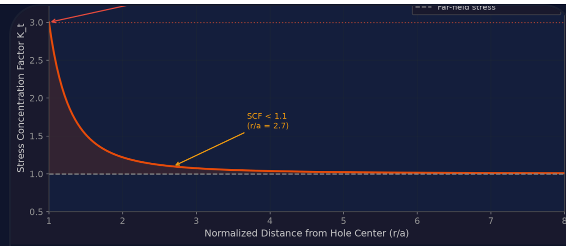

SCF decay curve — showing how stress concentration factor diminishes with distance from the hole edge, converging to the far-field nominal stress.

CROSS-VALIDATION

comparison

Three-method cross-validation — FEA vs analytical vs experimental results comparison.

Three-Method Validation

Comparing analytical (Kirsch), computational (FEA), and experimental (strain gauge) results quantifies the accuracy of each approach and reveals real-world error sources. Understanding *why* these methods disagree — and by how much — is more valuable than any single number.

Hand-derived Kirsch equations

Hand-derived Kirsch stress equations in polar coordinates

Numerical evaluation of Kirsch solution

Numerical evaluation with plate dimensions and loading

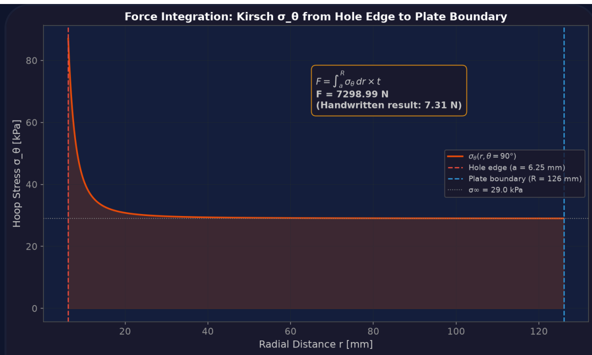

Force integration — verifying static equilibrium via stress integration

Analysis code output

Python analysis script output — stress profile computed along measurement line

Stress Analysis · FEA / Fusion 360 · Strain Gauges · Experimental Validation · Kirsch Solution · Elasticity

PROJECT 05

CNC Precision Machining — Production Portfolio

American Precision Machining — Mazak Integrex i-200 / Turning & Milling / Hurco

Production machining experience at American Precision Machining producing tight-tolerance components for industrial, hydraulic, and instrumentation applications. Operated multi-axis CNC equipment, programmed using conversational and G-code methods, and verified finished dimensions with calibrated metrology — routinely holding tolerances as tight as ±0.0005".

100%	±0.0005"	Ra 12.4	5-axis
QC PASS RATE	TIGHTEST TOLERANCE	BEST FINISH (MIN)	SIMULTANEOUS

MACHINED PARTS

Precision stainless steel components — machined to ±0.0005" tolerances with surface finishes to Ra 12.4 µin.

Four-Part Manufacturing Portfolio

Part A: Multi-threaded brass fitting body — three thread pitches, hex flange via live tooling, cross-drilled holes, ±0.0005" thread tolerances.

Part B: Stainless steel flanged hub — 6-hole bolt circle, round-to-hex transition, internal threading, perpendicularity ≤ 0.001".

Part C (Most Complex): Stainless steel hydraulic manifold block — internal cross-drilled passages, 6-face machining, multi-axis operations, O-ring glands. ☆☆☆☆☆ complexity.

Part D: Stainless steel open-window cage — thin-wall machining (0.125" wall), deflection management, concentricity to TIR ≤ 0.001".

Multi-Axis Machining Capability

Three CNC platforms operated for production:

- **Mazak Integrex i-200:** 5-axis simultaneous milling/turning, B-axis tilting spindle, C-axis polar milling
- **Mazak Turning & Milling Lathe:** Live tooling for secondary operations without re-fixturing
- **Hurco VMC:** 3-axis vertical milling with WinMax conversational programming

Programming: MAZATROL conversational, G-code (ISO 6983), GibbsCAM for complex 5-axis work.

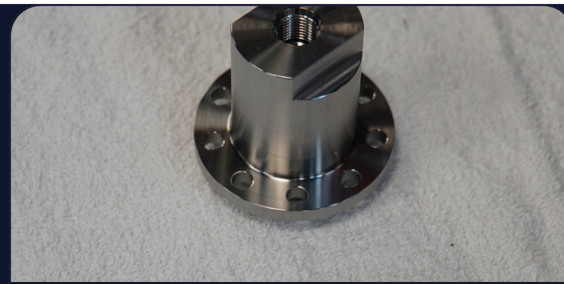

Additional machined components showing surface finish quality and geometric complexity.

Detail view — thread form quality and surface finish on a machined component.

Metrology & Inspection

10+ metrology instruments used across 40 dimensions on 4 parts:

- **CMM** for GD&T, true position, concentricity (18 features)
- **Mahr MarSurf XC 2** profilometer for Ra/Rz/Rq surface finish (20 measurements)
- Inside/outside/pitch/depth micrometers, digital calipers
- Thread plug and ring gages (Go/No-Go)
- Pin gages for precision bore verification
- Optical comparator for thread form inspection

Every dimension in spec: **40/40 conformance, 100%**

Surface Finish Science

Surface finish directly impacts sealing, wear, fatigue life, and corrosion resistance. Achieved Ra 12.4–36.4 µin across all parts — well within aerospace hydraulic component requirements. Theoretical finish predicted from cutting parameters ($f^2/8r$ formula), then verified with profilometry — demonstrating understanding of the relationship between machining parameters and surface quality.

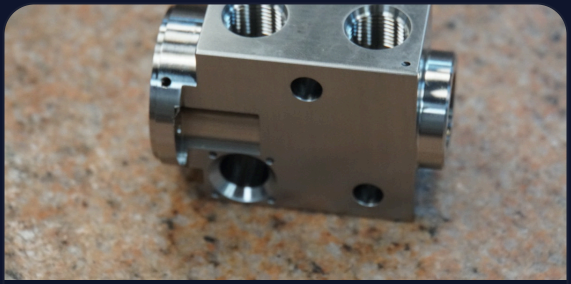

Surface finish closeup — face-milled stainless steel achieving Ra 12.4 µin (0.31 µm).

PROCESS CAPABILITY & TOLERANCE ANALYSIS

Process capability analysis — Cp/Cpk computed for critical dimensions across all four parts. Most features achieve Cpk > 1.5, with the tightest at Cpk ≥ 2.0.

Statistical Process Control

Cpk values computed from measurement data:

FEATURE	CP	CPK
Thread pitch diameter	≥ 1.25	≥ 1.25
OD dimensions	≥ 1.98	≥ 1.98
Bore ID	≥ 1.42	≥ 1.42

All Cpk values exceed the 1.33 industry standard for capable processes, with most above 1.5 (Six Sigma threshold).

Tolerance Stack Analysis

Worst-case tolerance consumption analyzed for assembly-critical dimension chains. RSS method applied to multi-feature tolerance stacks to determine statistical assembly clearance.

Understanding tolerance allocation is critical for manufacturing cost optimization — tighter than necessary tolerances add cost without functional benefit.

Tolerance stackup analysis — worst-case and RSS (root-sum-square) methods applied to assembly dimension chains.

Surface roughness comparison across surfaces

Surface roughness comparison across all measured surfaces

Inspection deviation analysis

Inspection deviation chart — measured vs nominal for all 40 features

Theoretical vs actual surface finish

Theoretical vs. measured surface finish validation

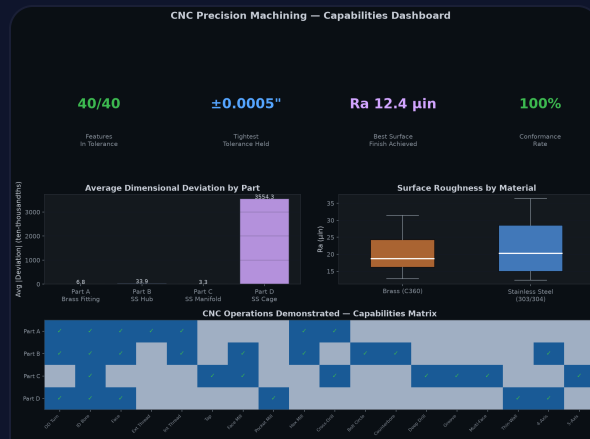

CNC operations capabilities dashboard

Tolerance consumption breakdown

Tolerance consumption across assembly feature chain

Measurement uncertainty budget

Measurement uncertainty budget — instrument, environmental, and operator contributions

Surface roughness parameter relationships

Ra/Rz/Rq parameter relationships across surface types

CNC Machining | 5-Axis | Metrology / CMM | GD&T / ASME Y14.5 | SPC / Cpk | MAZATROL | G-Code | GibbsCAM

PROJECT 06

Mortise Lock Reverse Engineering

Full Teardown → CAD Reconstruction → FDM Prototype

Complete reverse engineering of a commercial mortise lock — from systematic disassembly and precision measurement through parametric SolidWorks reconstruction and functional FDM 3D-printed prototype. A mechanically sophisticated system with ~10 interacting components in a compact volume.

10	10	6	Functional
COMPONENTS	SLDPRT FILES	PRINT ITERATIONS	PROTOTYPE

ASSEMBLY & MECHANISM

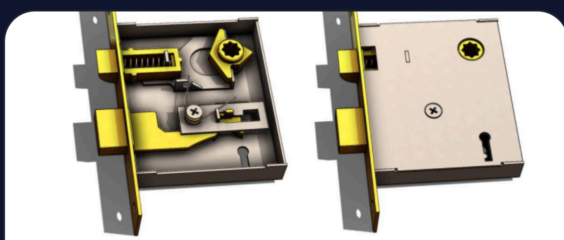

Mortise lock SolidWorks assembly — 10 components with full mate relationships enabling kinematic simulation of handle rotation and deadbolt throw.

Reverse Engineering Methodology

6-phase structured workflow: Disassembly → Measurement → CAD Modeling → Assembly → 3D Printing → Functional Validation.

- Systematic disassembly with component cataloging
- Digital caliper measurements (0.01mm resolution)
- Fully parametric SolidWorks models for all 10 components
- Assembly mates preserving actual kinematics (concentric, coincident, limit mates)
- FDM 3D printing with tolerance compensation (holes enlarged 0.2–0.4mm)

ENGINEERING ANALYSIS

Spring & Force Analysis

Derived the spring constant from geometry using the helical compression formula k = Gd&sup4;/($8D^3N_a$) = 3.96 N/mm. Computed preload force (10.10 N) and maximum working force (60.39 N).

Handle torque for latch retraction: 1.28 N·m — consistent with smooth, comfortable door handle operation.

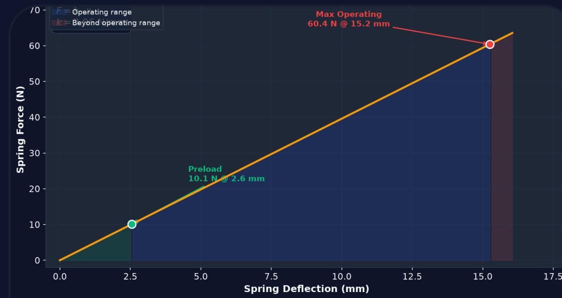

Latch return spring force analysis — Hooke's Law derivation from spring geometry, with Wahl factor correction for shear stress.

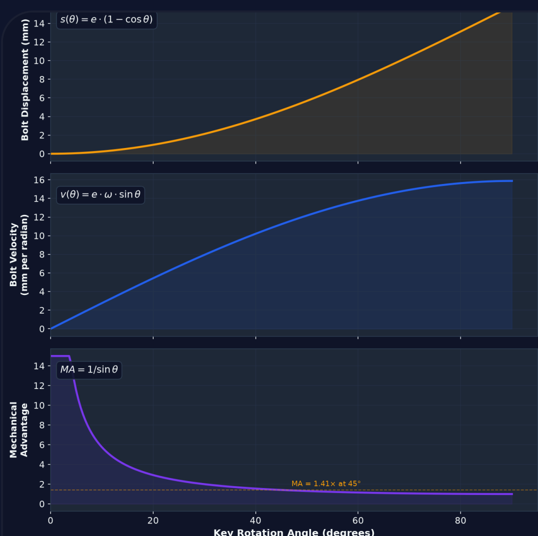

Cam displacement analysis — deadbolt throw (15.88mm) derived from eccentric cam geometry s(θ) = e(1 – cos θ).

Cam Kinematics — Deadbolt Actuation

The deadbolt cam converts ~90° of key rotation into 15.88mm of linear deadbolt travel. The displacement relationship $s(\theta) = e(1 - \cos\theta)$ reveals that mechanical advantage peaks at start ($\theta \to 0$) and diminishes as the cam approaches full extension.

Force amplification: $MA = 1/\sin\theta$ — a 50 N key force generates 70.7 N at the bolt at $\theta = 45°$.

Material Substitution Analysis

Quantified the performance trade-off when substituting PLA for steel:

- Steel deadbolt shear resistance: **30.0 kN** (6,740 lbf)
- PLA deadbolt shear resistance: **6.2 kN** (1,387 lbf)
- PLA latch bolt bevel angle increased from 15° to **25°** to compensate for higher PLA-on-steel friction ($\mu = 0.35$ vs 0.15)

PLA is a functional prototype material — sufficient for mechanism validation but requiring ~20% security margin reduction.

PLA bolt shear strength

Material substitution analysis — steel bolt (30 kN shear) vs. PLA bolt (6.2 kN shear), PLA provides ~20% of original security but validates mechanism function.

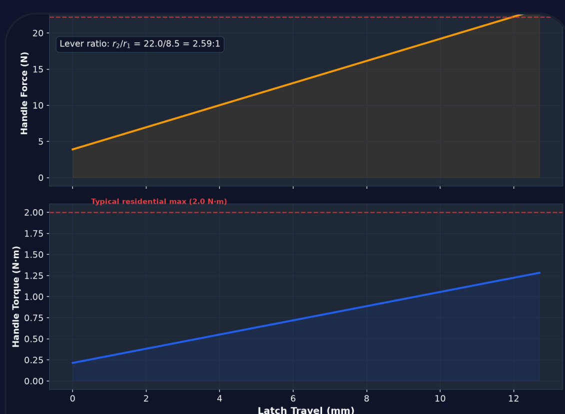

Handle force requirement curve — lever ratio reduces spring force from 60.39 N to 23.31 N at the handle, confirming comfortable operation.

Handle Ergonomics

The lever mechanism ratio (r_1/r_2) reduces the spring force experienced at the handle. Maximum handle force of 23.31 N — well below the 50 N threshold for comfortable prolonged operation. Handle torque: $T = F \times r_{handle} = 1.28$ N·m — smooth, effortless latch retraction.

CAD Accuracy Validation

Periodic comparison of CAD geometry against physical parts ensured model accuracy. Design intent preservation: nominal dimensions inferred from measurement clusters, tolerances estimated from measurement scatter. This process required inferring the designer's intent — not just copying geometry, but understanding why each feature is the size and shape it is.

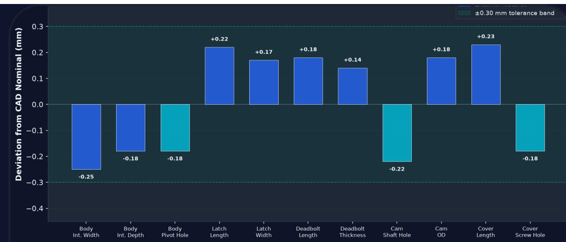

Dimensional accuracy analysis — CAD model vs. physical part measurements across all components.

Reverse Engineering | SolidWorks CAD | Mechanism Design | FDM 3D Printing | Cam Kinematics | Material Substitution

TECHNICAL SKILLS

Engineering Competencies

A cross-section of capabilities demonstrated across six projects — from CNC machining and CAD modeling to embedded systems and machine learning.

⚙

Manufacturing & CNC

- CNC Turning & Milling (3–5 axis)
- MAZATROL Conversational Programming

📊

Metrology & Quality

- CMM Operation & Programming
- GD&T (ASME Y14.5-2018)
- Process Capability (Cpk/SPC)

- G-Code (ISO 6983)
- GibbsCAM Multi-Axis
- Single-Point Threading
- Thin-Wall & Multi-Face Machining
- Blueprint Reading (ASME Y14.5)

- Surface Profilometry (Mahr MarSurf)
- Micrometer / Caliper / Pin Gage
- Thread Gaging (Go/No-Go)
- Measurement Uncertainty Analysis

CAD & Design

- SolidWorks Parametric Modeling
- Part & Assembly Design
- Reverse Engineering
- Design for Manufacturability (DFM)
- Tolerance Stack Analysis
- GD&T Callouts
- Engineering Drawings

Controls & Embedded

- PID Control (Tuning & Implementation)
- Sensor Fusion (Complementary Filter)
- Arduino / ATmega328P
- MATLAB / Simulink
- Real-Time Embedded Systems
- Stepper Motor Control (A4988)
- I2C / SPI / UART Communication

Analysis & Simulation

- FEA (Fusion 360)
- Fluid Dynamics (Bernoulli, Darcy-Weisbach)
- Structural Analysis (Lamé, Von Mises)
- Physics-Informed Neural Networks (PINN)

Tools & Software

- Python (PyTorch, NumPy, Matplotlib)
- SolidWorks + SolidWorks Flow Sim
- GibbsCAM
- Git / Version Control
- Microsoft Excel (Data Analysis)
- Arduino IDE

- Signal Processing (PPG, FFT, Filtering)
- Statistical Error Analysis
- FMEA (Failure Mode & Effects)

- Fusion 360 (CAD + FEA)

John Vallance

Mechanical Engineering — B.S. (Junior) | 2026

✉ johnvallance2@gmail.com

📞 (484) 632-6904